Mutant Rhodopsin Transgene Expression on a Null Background

Jeanne M. Frederick,[1] *Nataliia V. Krasnoperova,*[2] *Kirstin Hoffmann,*[4] *Jill Church-Kopish,*[1] *Klaus Rüther,*[4,5] *Kimberly Howes,*[1] *Janis Lem,*[2,3,6] *and Wolfgang Baehr*[1]

Purpose. To study mechanisms leading to photoreceptor degeneration in mouse models for autosomal dominant retinitis pigmentosa (adRP) based on the rhodopsin P23H mutation.

Methods. Mice of a transgenic line expressing a rhodopsin triple mutant, V20G, P23H, and P27L (GHL), were mated with rhodopsin (*rho*) knockout mice. Littermates of various ages and genotypes ($GHL^{+}rho^{+/+}$, $GHL^{+}rho^{+/-}$, and $GHL^{+}rho^{-/-}$) were examined for outer nuclear layer thickness and outer segment formation (histology), fate of mutant rhodopsin (immunocytochemistry), and photoreceptor function (electroretinogram; ERG).

Results. Mice expressing GHL-rhodopsin in the absence of wild-type rhodopsin had severe retinopathy, which was nearly complete by postnatal day (P)30. GHL-rhodopsin formed homodimers nearly exclusively on sodium dodecyl sulfate–polyacrylamide gel electrophoresis gels, whereas wild-type rhodopsin predominantly formed monomers. Expression level of mutant rhodopsin in predegenerate (P10) $GHL^{+}rho^{-/-}$ retinas was low, approximately 10% to 25% of normal levels. No elaboration of disc membrane or outer segment formation was observed at any time point examined. The mutant rhodopsin was found mostly in perinuclear locales (endoplasmic reticulum; ER) as evidenced by colocalization using the antibodies Rho1D4 and calnexin-NT.

Conclusions. GHL-rhodopsin dimerizes, localizes to the ER, and fails to transport and support outer segment formation. Additionally, the mutant protein does not support a scotopic ERG a-wave and accelerates photoreceptor degeneration over that occurring with the rhodopsin knockout alone. These findings indicate a cytotoxic effect of the mutant protein, probably elicited by an unfolded protein response. (*Invest Ophthalmol Vis Sci.* 2001;42:826–833)

From the [1]Moran Eye Center, University of Utah Health Science Center, Salt Lake City; the [2]Department of Ophthalmology and the [3]Molecular Cardiology Research Institute, New England Medical Center, Boston, Massachusetts; [4]Charité–Virchow Augenklinik, Humboldt University, Berlin, Germany; and the [6]Program in Genetics, Tufts University School of Medicine, Boston, Massachusetts.

[5]Present affiliation: Universitätsklinikum Eppendorf-Augenklinik, Hamburg, Germany.

Supported by Grants EY12008 (JL) and EY08123 (WB) from the National Eye Institute; Grant Ru 457/6-3 from Deutsche Forschungsgemeinschaft (KR); the Foundation Fighting Blindness (FFB; JL, WB); and a Center Grant of the FFB to the Department of Ophthalmology at the University of Utah. JL is the recipient of a Career Development Award and a James S. Adams Special Scholar's Award from Research to Prevent Blindness (RPB). WB is the recipient of a Senior Investigator Award from RPB.

Submitted for publication October 27, 2000; accepted December 8, 2000.

Commercial relationships policy: N.

Corresponding author: Jeanne M. Frederick, John A. Moran Eye Center, University of Utah Health Science Center, 50 North Medical Drive, Salt Lake City, UT 84132. jfrederi@hsc.utah.edu

Rhodopsin is an abundant, multifunctional intrinsic membrane protein, acting as a photoreceptor molecule; a rod outer segment (ROS) structural protein; and, in its activated form, as a guanosine triphosphate–guanosine diphosphate exchange factor.[1] More than 80 mutations in the human rhodopsin gene are associated with the genetically heterogeneous group of retinal degenerations referred to as retinitis pigmentosa (RP).[2–4] Rhodopsin mutants account for the largest proportion of autosomal dominant (ad) RP cases of known genetic origin (30%–40%).[5] The first rhodopsin mutation identified, P23H,[6] occurs most frequently in the United States. A transgenic mouse line bearing a single P23H mutation in the human rhodopsin gene accumulated mutant rhodopsin in the outer plexiform layer,[7] indicating misrouting of the mutant protein.[8] An independent transgenic mouse line expressing the rhodopsin mutations V20G, P23H, and P27L, produces a slowly progressing photoreceptor degeneration resembling human adRP.[9] It has been suggested that on the wild-type background, GHL mutant rhodopsin incorporated into ROS disc membranes, but basal discs appeared disorganized.[10] However, in vitro experiments, in which the P23H mutant protein was expressed in heterologous cells, showed low levels of expression and retention of the mutant protein in the ER.[11]

In transgenic mouse models, the mutant rhodopsin transgenes were expressed on wild-type genetic backgrounds in which normal rhodopsin was also expressed. Molecular mechanisms by which expression of mutant rhodopsin leads to photoreceptor cell death explaining the dominant phenotype of retinal degeneration are not understood. Availability of rhodopsin knockout mice[12,13] has made it possible to study mutant rhodopsin expressed in vivo isolated from wild-type rhodopsin. We generated mice expressing GHL-rhodopsin on $rho^{-/-}$, $rho^{+/-}$, and $rho^{+/+}$ backgrounds, compared the rates of retinal degeneration, determined whether the mutant protein alone was capable of supporting ROS formation, and localized the mutant protein. Severity of retinal degeneration was determined by the ratio of mutant to wild-type protein. The most severe disease phenotype occurred when the GHL transgene was expressed in the absence of wild-type rhodopsin. We were surprised to observe that the mutant rhodopsin alone was unable to support disc membrane or outer segment formation. Immunogold labeling of $GHL^{+}rho^{-/-}$ retina sections revealed mutant rhodopsin localized to perinuclear regions of the rod, together with calnexin, a resident ER protein and chaperone. These results are interpreted to suggest that the misfolded, nonfunctional mutant rhodopsin accumulates in the ER, a condition known to elicit unfolded protein response (UPR; reviewed in Reference 14), leading to apoptosis.

Methods

Genotyping

Transgenic and knockout mice were cared for in accordance with the ARVO Statement for the Use of Animals in Ophthalmic and Vision Research and the guidelines of the University of Utah Committee on Animal Research. The transgene and wild-type rhodopsin gene were

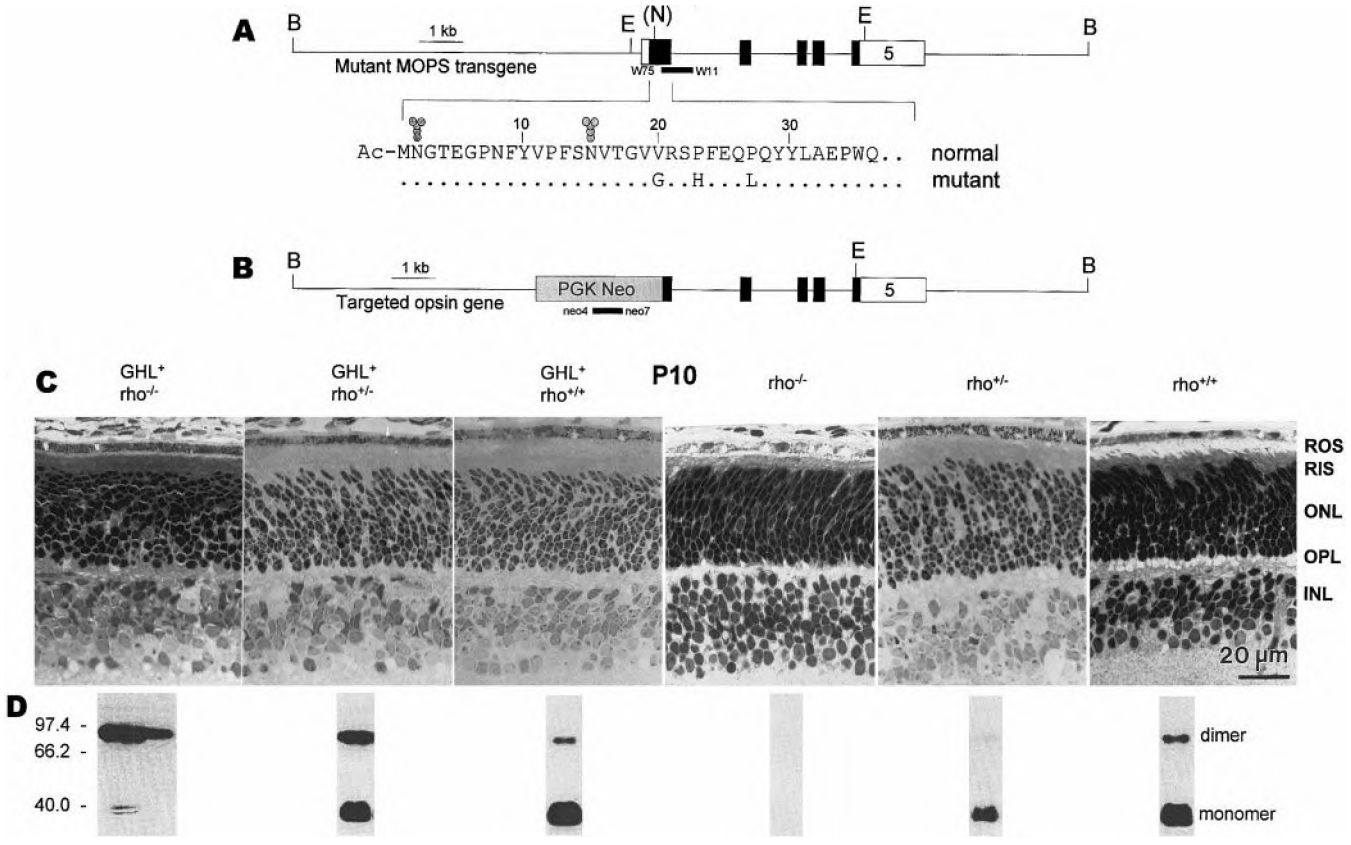

FIGURE 1. Transgene, targeted rhodopsin gene, P10 histology and immunoblot analysis. (**A**) Mouse rhodopsin transgene containing mutations in exon 1. N, A deleted *Nco*I site, the restriction fragment length polymorphism (RFLP) used to identify GHL$^+$ mice. *Underneath*, N-terminal sequence of mouse rhodopsin and amino acid substitutions (G, H, L) of the transgene. N_2 and N_{15} are glycosylated in mature rhodopsin. (**B**) Targeted rhodopsin gene. The first 111 codons of exon 1, including the translational start, were replaced by a neomycin gene.[13] (**C**) Retinas of four littermates and age-matched *rho*$^{-/-}$ and *rho*$^{+/+}$ mice show comparable histology at day P10. Sections were stained with 1% methylene blue/azure II in sodium borate solution and photographed in superior regions equidistant from the optic nerve. RIS, rod inner segments; OPL, outer plexiform layer. Bar, 20 μm. (**D**) Immunoblot of P10 retina extracts probed with a C-terminus–directed mAb, Rho1D4. Six panels are from one blot, partitioned to illustrate with corresponding histology. Wild-type rhodopsin migrated predominantly as a monomer (40 kDa, *rightmost panel*), whereas the transgene product formed a dimer almost exclusively when isolated from wild-type rhodopsin (GHL$^+$*rho*$^{-/-}$, *leftmost panel*). Two monomeric species were visible faintly only when the sample was overloaded (*lane 1, first panel*). As expected, the *rho*$^{-/-}$ retinal extract was negative (*fourth panel from left*).

distinguished by differential restriction digestion of a 1.3-kb amplification product produced by primers W75 (5′-AGACTGACATGG GGAGGAATTC-3′) and W11 (5′-GTGCCTGTGATCACAGCACTT-3′).[9] The presence of the targeted rhodopsin gene was detected by separate amplification of a 493-bp fragment from the neomycin (*Neo*) gene using primers Neo4 (5′-CGGGAGCGGCGATACCGTAAAGC-3′) and Neo7 (5′-GAAGCGGGAAGGGACTGG CTGCTA-3′).

Immunoblot Analysis of Transgene Expression Level

Retinas from postnatal day (P)10 mice were isolated in ice-cold phosphate-buffered saline (PBS), placed in tubes individually, frozen in liquid nitrogen, and kept at −80°C until used. Solubilization of retinas was achieved using a two-buffer process. To each tube, 92 μl of buffer 1 (2.8% sodium dodecyl sulfate [SDS]; 15 μg/ml each of pepstatin, leupeptin, aprotinin; 0.1 mM phenylmethylsulfonyl fluoride [PMSF], and 2 mM EDTA in 0.09 M Tris-HCl [pH 6.8]) was added. The retinas were vortexed, allowed to rest for 1 minute, revortexed, and allowed to rest 20 minutes at room temperature. Then, 40 μl of buffer 2 (0.4% bromophenol blue and 4.7% β-mercaptoethanol in 9.4% glycerol) and 8 μl of 10 mM Tris-HCl (pH 7.4) were added per tube, for a total volume of 140 μl per retina, at room temperature. Retinal homogenates of the same genotype and age were pooled, producing the stock for subsequent dilutions. Samples shown in Figure 1D contained 1:70 retina per lane, with the exception of GHL$^+$*rho*$^{-/-}$, which contained 1:14 (Fig. 1, set 1, lane 1), 1:140 (lane 2), and 1:70 retina (lane 3). Proteins were separated using 12.5% sodium dodecyl sulfate–polyacrylamide gel electrophoresis (SDS-PAGE; 50 minutes, 200 V),[15] transferred electrophoretically onto nitrocellulose membrane (1 hour, 100 V), and probed using monoclonal antibody (mAb) Rho1D4[16] (1:750) for 3 hours at room temperature.

Microscopy

For light and electron microscopy, right eyes were processed initially, as described.[17] Thin (silver-gold) sections were cut from selected blocks, placed on Formvar- (SPI, West Chester, PA) and carbon-coated slot grids, stained by uranyl acetate followed by lead citrate, and examined with an electron microscope (H-600; Hitachi, Brisbane, CA) at 75 kV. For light microscope immunocytochemistry, left eyes were fixed using freshly prepared 4% paraformaldehyde in 0.1 M phosphate buffer (pH 7.4) and cryoprotected using 30% sucrose in buffer. Mouse mAb Rho1D4 (1:500, 25 μl), directed against the C terminus of rhodopsin, was applied to each 12-μm-thick section. Peanut agglutinin (5 μg/ml, Texas red–conjugated) was co-incubated with the secondary antibody to demonstrate extracellular cone sheaths. Sections were photographed using a confocal microscope (LSM 510 inverted Laser Scan; Carl Zeiss, Thornwood, NY).

Electron Microscopic Immunocytochemistry

Nonosmicated P10 and P15 retinas were selected for immunocytochemistry using antibody Rho1D4 in a postembedding procedure. Thin sections were cut, placed on slot grids, etched 30 minutes with a 10% hydrogen peroxide solution, rinsed twice with 5 ml deionized water and once with Tris saline (0.1 M Tris-HCl, 0.87% NaCl [pH 7.5]). Blocking was achieved by incubating 1 hour in 10% normal goat serum in a solution of 0.1 M Tris-HCl, 0.5% Triton, 0.5% bovine serum albumin (BSA). The grids were washed with 10 ml Tris saline, then incubated 1 to 2 hours at room temperature in 25 μl of primary antibody (diluted 1:25) in Tris-Triton-BSA. After they were rinsed drop-wise with 15 ml Tris saline, the grids were incubated 1 hour in 15 nm gold-conjugated goat anti-mouse IgG (catalog number 15747; Ted Pella, Redding, CA) diluted 1:75 in Tris-Triton-BSA. The grids were washed in Tris saline, fixed 10 minutes in 0.1% glutaraldehyde-0.1 M Tris saline-Triton, rinsed in buffer followed by water, dried, and stained. Companion grids of each specimen were processed in parallel, omitting incubation in primary antibody, as negative controls. Inner nuclear layer (INL) and inner plexiform layer (IPL) regions (internal negative control) of each section were also examined to establish background levels of label. Application of the N-terminus–directed mAb Rho4D2[1] to companion grids rendered identical localizations of weaker signal strength (not shown).

Colocalization of calnexin and GHL-rhodopsin was achieved by simultaneous incubation with primary antibodies. Thin sections of P10 *rho*$^{-/-}$ and GHL^{+}*rho*$^{-/-}$ retinas were placed on Formvar- (SPI) and carbon-coated gold slot grids. Calnexin-NT (catalog number SPA-865; StressGen Biotechnologies, Victoria, British Columbia, Canada), an antipeptide polyclonal antibody directed toward residues 50-68 of canine calnexin,[18] was applied to sections for 1 hour before addition of Rho1D4 for 1 hour. After they were rinsed, the sections were incubated in Tris-Triton-BSA containing 5 nm gold-conjugated goat anti-rabbit IgG (catalog number 15725; Ted Pella) to detect calnexin-NT and 15 nm gold-conjugated goat anti-mouse IgG to detect RholD4.

Electroretinograms

Pupils of dark-adapted mice were dilated using 1% atropine-0.5% tropicamide, and animals were anesthetized subcutaneously with 20 mg xylazine and 40 mg ketamine per kilogram body weight. Electroretinograms (ERG)s were recorded using a monopolar corneal contact lens electrode (Medical Workshop, Groningen, The Netherlands). Silver reference and neutral electrodes were placed subcutaneously 3 mm below the eye and in the forehead, respectively. Mice were placed into a Ganzfeld bowl (Toennies Multiliner Vision, Hőchberg, Germany). The Ganzfeld stimulus was a white flash with a color temperature of 6000° K and 50-μsec duration. For the scotopic ERG, eight flash energies from 4×10^{-5} candelas (cd)/m^2 to 1 cd/m^2 were used. Because of the partly severe reduction of the rod responses, only the maximal scotopic ERG response (1 cd/m^2) is presented. Two responses were averaged (interstimulus interval, 5 seconds). The curve was smoothed by a low-pass filter to obtain the b-wave minus oscillatory potentials. The oscillatory potentials were then recorded in a separate step using a 100- to 1000-Hz band-pass filter. For the photopic ERG, a 30-cd/m^2 background light was used. A single-flash response to a 15-cd/m^2 light flash was recorded (average of 16). Scotopic and photopic ERGs were repeated three times during each session to confirm stability. Final amplitude values were the mean of three determinations.

Results

Onset of Retinal Degeneration in GHL^{+}*rho*$^{-/-}$ Mice

To measure severity of retinal degeneration in various genotypes, outer nuclear layer (ONL) thickness was compared with ONL thickness in age-matched normal mice (approximately 10–12 rows of photoreceptor nuclei in adult mice). Matings were arranged between GHL^{+}*rho*$^{+/-}$ and *rho*$^{+/-}$ parental mice, agouti in pigmentation, to produce littermates expressing the mutant transgene on all backgrounds. One hundred twenty mice ranging in age from P10 to 7 months (P210) were examined. Inheritance followed Mendelian patterns—that is, the GHL transgene (Fig. 1A) was transmitted to approximately 50% of progeny, whereas the neomycin gene (Fig. 1B), indicating presence of the rhodopsin knockout alleles, was transmitted to approximately 75% of pups. For all genotypes, the ONL and photoreceptor inner segments developed normally through P10 (Fig. 1C). Onset of degeneration in GHL^{+}*rho*$^{-/-}$ mice occurred between P10 and P15, roughly coinciding with eye opening (P12), a time when rhodopsin gene expression significantly increases.[19] Autophagic vacuoles were observed ultrastructurally in P10 GHL^{+}*rho*$^{-/-}$ retinas, although the ONL thickness still consisted of 10 rows.

Mutant and Wild-Type Rhodopsin Expression in Predegenerate Retina at P10

Previous experiments measuring RNA levels indicated that the GHL transgene contributed approximately 50% of total rhodopsin RNA in GHL^{+}*rho*$^{+/+}$ retina.[9] To estimate the amount of mutant rhodopsin in predegenerate GHL^{+}*rho*$^{-/-}$ retinas, Western blots were produced from P10 retinas of each genotype (Fig. 1D). Dimer formation of normal rhodopsin is thought to result from temperature- and SDS-dependent aggregation during retinal extract preparation.[20] In contrast to normal rhodopsin, GHL-rhodopsin migrated predominantly as a dimer, whereas only trace amounts of monomeric species of GHL-rhodopsin were present (Fig. 1D, left lane). Scanning densitometry of two independent blots (not shown) estimated the amount of mutant rhodopsin produced in GHL^{+}*rho*$^{-/-}$ retinas to be 10% to 25% of wild-type values, or significantly less than predicted from RNA levels,[9] suggesting that the mutant protein had a shorter half-life than normal rhodopsin (assuming equal translation rates of mutant and normal mRNAs). The results are consistent with an altered, less stable structure of mutant rhodopsin that defaults into a dimer in the presence of SDS.

Comparative Histopathology

Because ERG responses can be measured reliably in P30 mice, we assessed retina disease in littermates of this age. Consistent with earlier findings,[13] the number of rows of photoreceptor nuclei in *rho*$^{-/-}$, *rho*$^{+/-}$, and *rho*$^{+/+}$ mouse retinas were 9 to 10, 10, and 10 rows, respectively (Figs. 2D, 2E, 2F). Retinas of these genotypes are distinguished by their differences in length of ROSs, which were absent in *rho*$^{-/-}$ mice and were approximately 80% of wild-type length in *rho*$^{+/-}$ mice. In contrast, the ONL of GHL^{+}*rho*$^{-/-}$ retinas were reduced to one to three rows of nuclei with no ROSs (Fig. 2A). GHL^{+}*rho*$^{+/-}$ retinas revealed 4 to 5 rows of photoreceptor nuclei with severely truncated ROSs (Fig. 2B), whereas GHL^{+}*rho*$^{+/+}$ retinas exhibited 10 rows of photoreceptor nuclei with somewhat (40%) shortened ROSs (Fig. 2C). Thus, expression of the mutant transgene on the *rho*$^{-/-}$ background resulted in loss of approximately 80% of photoreceptor cells by P30.

Ultrastructurally, disorganization of the basal discs was evident in GHL^{+}*rho*$^{+/+}$ rods, and misoriented packets of disc membrane were present in the interphotoreceptor matrix (Fig. 2I), indicating failed incorporation of nascent discs. *Rho*$^{+/-}$ retina revealed mildly disorganized outer segments (Fig. 2K). GHL^{+}*rho*$^{+/-}$ retina displayed severely shortened ROSs (Fig. 2H) and debris-filled vacuoles in inner segments (not shown). *Rho*$^{-/-}$ retina revealed no disc membranes but, rather, connecting cilia ending abruptly in the interphotoreceptor matrix (due to plane of section; Fig. 2J) or in terminal sacs. Sacs containing tubules, membrane stacks, mitochondria, and/or

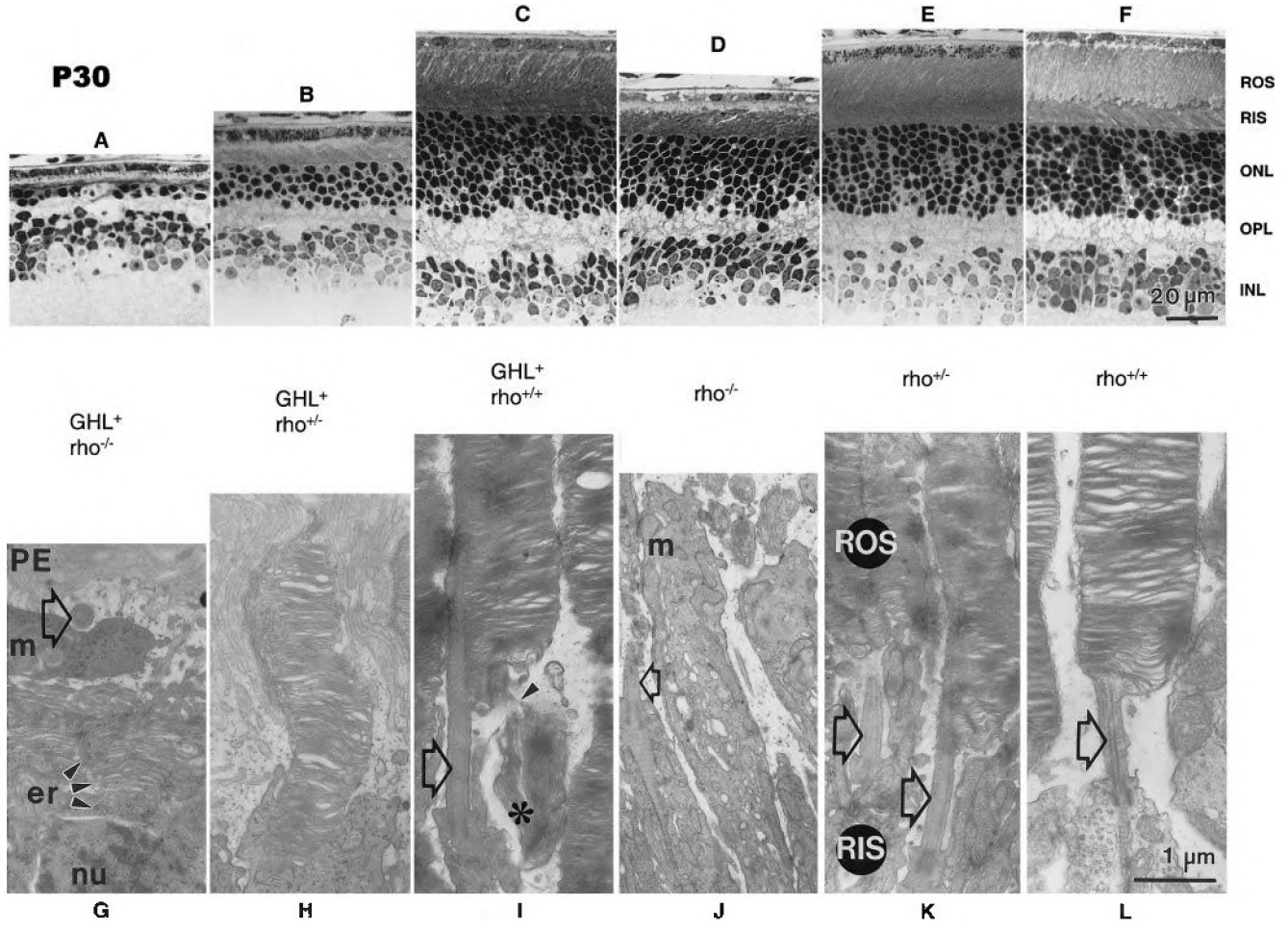

FIGURE 2. Retinal histology of P30 littermates. Light micrographs. Transgene expression on null or haploid backgrounds revealed reduced ONL thicknesses (**A**, **B**). Conversely, presence of normal rhodopsin retarded the rate of degradation of rods that express the transgene (**B**, **C** compared with **A**). (**G** through **L**) Rod photoreceptor ultrastructure of phenotypes corresponding to (**A**) through (**F**). *Open arrows*: Connecting cilia. Transgene expression resulted in absent ROSs (**G**, $rho^{-/-}$ background), severely shortened ROSs (**H**, $rho^{+/-}$ background), and packets of disc membrane (**I**, $rho^{+/+}$ background, ✻) apparently being sloughed near the ROS bases. *Arrowhead*: Site of membrane connection. Mitochondria were present in the inner segment of $rho^{-/-}$ retina (**J**, m), but mitochondria were scarce in $GHL^{+}rho^{-/-}$ retina (**G**) where endoplasmic reticulum (er) formed concentric stacks surrounding the rod nucleus. PE, retinal pigmented epithelium; nu, nucleus.

ribosomes were also observed in the matrix. $GHL^{+}rho^{-/-}$ rods were characterized by absence of outer segments, apparent sloughing of inner segment organelles (Fig. 2G, m) in sacs, and redundancy of ER (Fig. 2G, arrowheads). The redundancy of ER membrane is reminiscent of overproduction of ER cisternae in dominant rhodopsin mutants of *Drosophila melanogaster.*[21] These results show that GHL-rhodopsin perturbed ROS formation when wild-type rhodopsin was present, but did not support ROS formation when normal rhodopsin was absent.

Rhodopsin Immunolocalization

Confocal immunolocalization was performed to assess the subcellular distribution of GHL-rhodopsin at P10 and at P30 with mAb Rho1D4. At P10, retinas expressing GHL-rhodopsin (Figs. 3D, 3E, 3F) had ONL thicknesses nearly equivalent to those of $rho^{-/-}$, $rho^{+/-}$, and $rho^{+/+}$ retinas (Figs. 3A, 3B, 3C). However, comparison of Rho1D4 labeling on genetic backgrounds of two (Fig. 3F), one (Fig. 3E), or zero (Fig. 3D) wild-type rhodopsin alleles revealed progressive restriction of label to perinuclear regions of the proximal ONL. Thus, genetic removal of wild-type rhodopsin appeared to restrict the distribution of expressed transgene product in $GHL^{+}rho^{-/-}$ retina (Fig. 3D). Later, P30 $rho^{+/-}$ and $rho^{+/+}$ retinas revealed preferential ROS labeling (Figs. 3H, 3I), whereas $rho^{-/-}$ retinas were negative (Fig. 3G). In a $GHL^{+}rho^{+/+}$ littermate retina, label was found mostly in truncated ROSs, but also in inner segments and perinuclear regions (Fig. 3L). Relative to that of a $rho^{+/-}$ littermate (Fig. 3H), the ONL thickness of a $GHL^{+}rho^{+/-}$ retina was halved, and immunolabel was detectable in perinuclear regions and severely truncated ROSs (Fig. 3K). Compared with P10 (Fig. 3D), $GHL^{+}rho^{-/-}$ retina at P30 exhibited only slight labeling, because rapid degeneration had reduced the ONL thickness to one to three nuclear rows (Fig. 3L). Cones were apparently spared from degeneration at P30, as evidenced by peanut agglutinin binding to extracellular cone sheaths, consistent with human RP phenotypes in which degenerative effects target rods initially. Collectively, these results suggest retention of GHL-rhodopsin, followed by degradation and rod degeneration.

Absence of ROS Membrane in Retinas Expressing GHL-Rhodopsin on a Null Background

To determine the subcellular fate of mutant rhodopsin more precisely, immunogold-labeling experiments were performed at the electron microscopic level. No ROS formation was de-

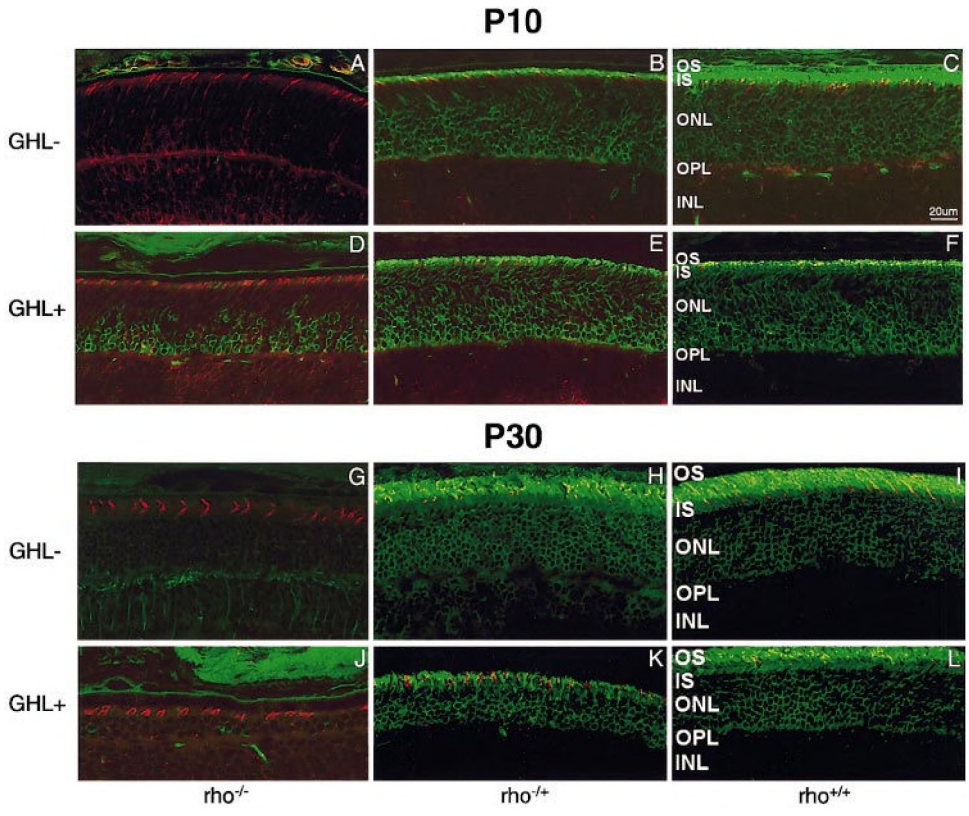

FIGURE 3. Localization of fluorescein isothiocyanate (FITC)–labeled rhodopsin (*green*) versus binding of peanut agglutinin (*red*) in P10 age-matched mice (**A** through **F**) and P30 littermates (**G** through **L**). Rho1D4 recognized the C termini of wild-type and mutant rhodopsins in rod photoreceptors; peanut agglutinin binding revealed cone sheaths. Rho1D4 (1:500 dilution) was incubated with cryostat sections for 1 hour at room temperature. After they were rinsed, the sections were incubated with fluorescein-conjugated rabbit anti-mouse secondary antibody (1:100) and were photographed using a confocal microscope (×40 oil objective, optical slice 1.3 μm). *Rho*$^{-/-}$ retinas were nonreactive with Rho1D4 antibody, consistent with deletion of the rhodopsin gene (**A**). In the ONL of P10 GHL^{+}*rho*$^{-/-}$ retina (**D**), rod perinuclear regions were specifically immunolabeled. Labeling of P10 *rho*$^{+/+}$ retina (**C**) was, in contrast, predominantly that of ROS. Labeling of P30 *rho*$^{+/+}$ retina (**I**) was that of ROS, whereas P30 GHL^{+}*rho*$^{-/-}$ retina (**J**) showed slight specific label, owing to degeneration. FITC-fluorescence associated with sclera and capillaries of the OPL and choroid was nonspecific background. OS, outer segment; IS, inner segments.

tected in P10 GHL^{+}*rho*$^{-/-}$ retina (Fig. 4A). However, label was seen immediately external to the nuclear envelope or in the narrow interval between rod nuclei (Fig. 4B). ROS membrane in P15 wild-type rods (Figs. 4D, 4E) is compared with the absence of ROS membrane in a GHL^{+}*rho*$^{-/-}$ littermate retina (Figs. 4C, 4F). When the transgene was expressed in the absence of wild-type rhodopsin, clusters of immunogold label were observed near or between rod nuclei and in close proximity to rough ER (Figs. 4B, 4G). The perinuclear region contains ER membrane, into which nascent polypeptide chains are translocated. It is notable that the dense gold particle clusters were observed only over photoreceptors and only in specimens expressing the mutant protein. In contrast, a *rho*$^{+/+}$ ROS examined under high-power magnification showed widespread, diffuse gold particle distribution that is typical of wild-type rhodopsin immunoreactivity (Fig. 4E). Specific labeling, as well as disc membrane, was absent in a comparable GHL^{+}*rho*$^{-/-}$ rod (Fig. 4F). Despite thorough searches at P10

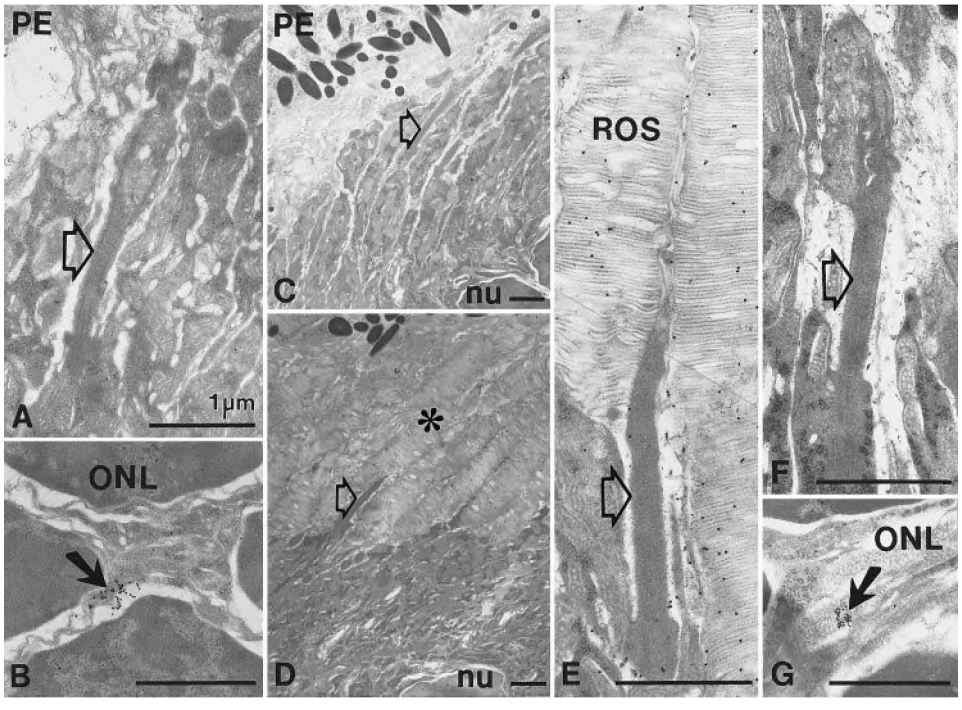

FIGURE 4. Electron microscopic immunolocalization of transgene product in GHL^{+}*rho*$^{-/-}$ mice. (**A**) Micrograph showing absence of ROS membrane and presence of a small sac distal to a connecting cilium (*arrowhead*) in P10 GHL^{+}*rho*$^{-/-}$ retina. (**B**) Labeling of membrane situated between two P10 rod nuclei using Rho1D4 (*arrow*). (**C**) Low-power micrograph showing inner segments but absence of ROS disc membrane in P15 GHL^{+}*rho*$^{-/-}$ retina. (**D**) Low-power micrograph showing, in contrast, extent of ROS (✻) development in P15 *rho*$^{+/+}$ littermate. (**E**) Rho1D4 labeling of ROS membrane in P15 *rho*$^{+/+}$ retina. (**F**) In P15 GHL^{+}*rho*$^{-/-}$ retina, connecting cilia were observed to end abruptly or in a membrane-containing sac; two gold particles overlying this example of a terminal sac are insignificant label over background levels. (**G**) Gold particle cluster (*arrow*) in perinuclear region of P15 GHL^{+}*rho*$^{-/-}$ rod. PE, retinal pigmented epithelium; nu, nucleus.

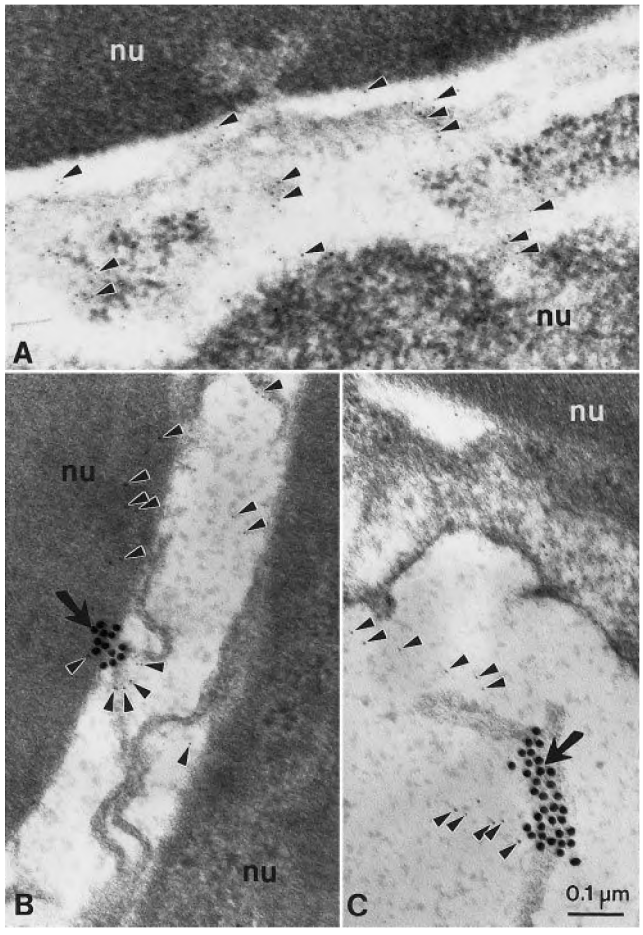

FIGURE 5. Colocalization of calnexin and GHL-rhodopsin. Calnexin, an ER integral membrane protein, binds transiently to many newly synthesized glycoproteins. Calnexin exhibits prolonged binding to misfolded or incompletely folded proteins.[34] GHL-rhodopsin contains N-linked glycosylation sites at N_2 and N_{15}, and would be predicted to interact directly with calnexin. (**A**) Immunogold (5 nm; *arrowheads*) showing localization of calnexin perinuclearly in P10 $rho^{-/-}$ photoreceptors. Colocalization (**B**, **C**) of Rho1D4 (15-nm gold, *arrows*) and calnexin (5-nm gold, *arrowheads*) is shown in P10 $GHL^{+}rho^{-/-}$ rods.

(Fig. 4A), P15 (Fig. 4F), and P30 (Fig. 2G), conventional ROSs were never observed in $GHL^{+}rho^{-/-}$ retinas.

GHL-Rhodopsin Colocalizes with Calnexin in ER

Calnexin, an ER integral membrane protein and lectinlike chaperone that recognizes $Glc_1Man_9GlcNAc_2$ oligosaccharide, transiently and selectively binds to nascent glycoproteins.[22,23] Direct interaction of nascent polypeptide with calnexin may occur if glycans are present within approximately 50 residues of a protein's N terminus.[24] Use of an anti-calnexin antibody directed toward its N terminus showed that in $rho^{-/-}$ retina, calnexin localized to perinuclear locales corresponding to the ER (Fig. 5A). In predegenerate P10 $GHL^{+}rho^{-/-}$ retina, calnexin and Rho1D4 (GHL-rhodopsin) were observed to colocalize (Figs. 5B, 5C). Further, the mutant rhodopsin label appeared to cluster or aggregate consistent with the protein's tendency to form homodimers, even in the presence of SDS (Fig. 1D). These results are consistent with accumulation of misfolded nascent protein in the ER.

Progression of Retinal Degeneration up to P210

To summarize the relative degeneration rates, ONL thicknesses were plotted as a function of time. In $GHL^{+}rho^{+/+}$ retinas, the rod degeneration was slow but complete by P210 (Fig. 6A). When both normal rhodopsin alleles were absent, the degeneration was much faster and essentially complete at P60. Degenerations in $rho^{-/-}$ and $GHL^{+}rho^{+/+}$ retinas progressed at nearly the same rate. $Rho^{-/-}$ rods, however, never formed an outer segment, whereas $GHL^{+}rho^{+/+}$ rods did. To correlate ONL thickness with function, ERGs from individual $rho^{-/-}$ and $rho^{+/-}$ mice, as well as $GHL^{+}rho^{-/-}$ and $GHL^{+}rho^{+/+}$ mice were studied as a function of age. Transgene expression on a null background led to an early and severe loss of rod function; scotopic (rod) ERG a- and b-wave amplitudes of the P30 $GHL^{+}rho^{-/-}$ mouse were not recordable, consistent with absence of ROSs.[17] Decay of ERG b-wave amplitudes as a function of age up to P180 is summarized for scotopic (Fig. 6B) and photopic (Fig. 6C) conditions. Scotopic b-wave responses of $rho^{-/-}$ mice vanished at P90. Decline of scotopic responses of $GHL^{+}rho^{+/+}$ mice was slower, with a well detectable response at P90. In contrast, scotopic responses of heterozygotes attained a high level, even at P180, and thereafter showed a moderate decline. The photopic response of the $GHL^{+}rho^{-/-}$ mouse, most likely reflecting cone activity, was barely detectable at P30. Decay of $rho^{-/-}$ and $GHL^{+}rho^{+/+}$ photopic responses occurred at similar rates. The results show that mitigation of degeneration occurring with GHL transgene expression was correlated with wild-type rhodopsin gene copy number. Overall, degeneration occurred with the following

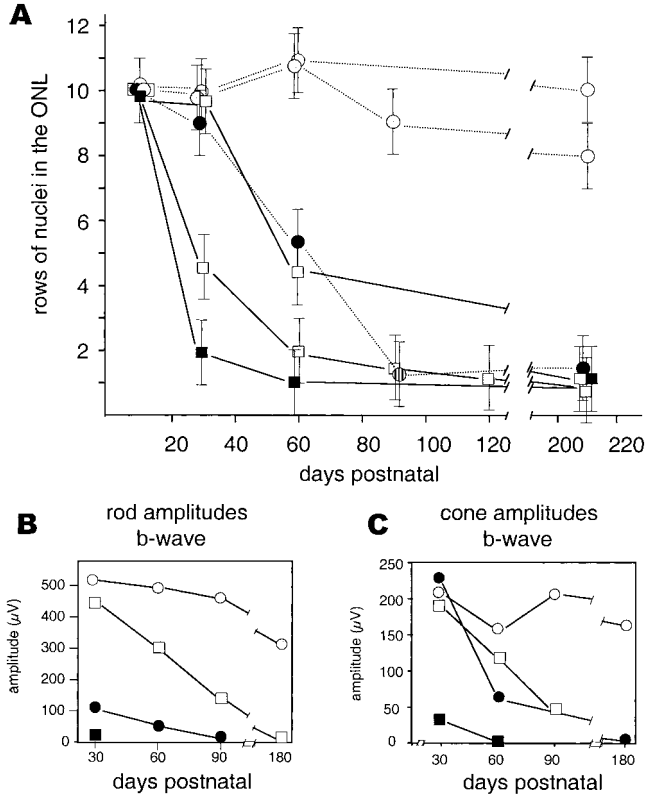

FIGURE 6. Progression of retinal degeneration with age and correlative ERGs. (**A**) Plot of ONL thicknesses versus time in age-matched mice. Genotypes are indicated as follows: (○) $Rho^{+/+}$; (◍) $rho^{+/-}$; (●) $rho^{-/-}$; (□) $GHL^{+}rho^{+/+}$; (▨) $GHL^{+}rho^{+/-}$; and (■) $GHL^{+}rho^{-/-}$. (◍) represents a data point derived from Figure 4C (*right*) in Reference 13. Each other data point derives from four or more mice generated in this study. (**B**) Plot of scotopic (rod-dominated) b-wave amplitudes versus time (stimulus strength, 1 cd/m^2), measured from littermates. (**C**) Plot of photopic (cone) b-wave amplitudes versus time (stimulus strength, 15 cd/m^2), recorded from littermates. Symbols in (**B**) and (**C**) defined as in (**A**).

order of severity: GHL$^+$*rho*$^{-/-}$ > GHL$^+$*rho*$^{+/-}$ > *rho*$^{-/-}$ ~ GHL$^+$*rho*$^{+/+}$ > *rho*$^{+/-}$ > *rho*$^{+/+}$.

Discussion

From our study of GHL-rhodopsin expressed in vivo on a null background, we derive several conclusions. First, GHL-rhodopsin misfolds and fails to achieve its mature form. Evidence for this stems from its preferential dimer formation (Fig. 1), its association with calnexin (Fig. 5), and its containing P23H, which has been shown previously to misfold in vitro.[25] The half-life of the mutant protein is apparently shorter than that of wild-type rhodopsin, because GHL-rhodopsin accounted for much less than 50% of total rhodopsin. Alternatively, attenuated translation of mutant mRNA may account for the low protein level. Folding of the nascent polypeptide chain is most likely facilitated by ER luminal chaperones with proline peptidyl cis-*trans* isomerization (PPI) activity, as has been shown for R_1-R_6 rhodopsin in *Drosophila*[26] and for red-green pigments by Ferreira et al.[27] As a consequence of mutation, luminal chaperones with PPI activity are most likely unable to assist in correct folding of the nascent chain. The dimer formation on SDS-PAGE is reminiscent of that observed in *Drosophila* ninaE^{D1} mutants, attributed to arrest in wild-type rhodopsin maturation due to absence of a rhodopsin-specific chaperone.[28] The existence of dimeric mutant rhodopsin or higher aggregates in situ cannot be confirmed. However, immunogold clusters associated specifically with the GHL mutant (Figs. 4B, 4G; 5B, 5C), but absent in wild-type rods, may reflect aggregation of GHL-rhodopsin.

Second, once synthesized, the mutant protein is retained in the ER. In P10 GHL$^+$*rho*$^{-/-}$ retinas, intense rhodopsin-specific immunolabel was observed in perinuclear locales (Fig. 3). Further, the predominant perinuclear localization coincided with calnexin localization. *Rho*$^{+/+}$ and *rho*$^{+/-}$ retinas also exhibited perinuclear labeling, but only slightly, consistent with ongoing biosynthesis and transport to the ROS. Compartmentalization of mutant rhodopsin in nondisc membranes was inferred by early observation that extraction of GHL$^+$*rho*$^{-/-}$ retinas with 1% octylglucoside (a detergent that dissolves disc membranes readily) before SDS-PAGE failed to detect any mutant rhodopsin, whereas wild-type rhodopsin was readily detectable (not shown). Retention of GHL-rhodopsin would prevent its subsequent transport to and through the connecting cilium to support outer segment formation, a key role of normal rhodopsin.

Third, severity of retinal degeneration occurring with transgene expression is inversely correlated with wild-type rhodopsin gene copy number. As shown in Figure 6, the degeneration was most severe in the absence of wild-type alleles, moderate in the presence of one wild-type allele, and least severe in the presence of two wild-type alleles. Although retinas from P30 *rho*$^{+/-}$ mice were nearly identical with those of *rho*$^{+/+}$ mice and showed no decrease in ONL thickness (Figs. 2E, 2F), transgene expression on a *rho*$^{+/-}$ background resulted in a 50% reduction in ONL thickness (Fig. 2B). In *rho*$^{+/-}$ mice, the ONL thickness was reduced by approximately 10% at P90 and by approximately 20% at P180 (Lem et al., unpublished results, 1998). Consequently, the 50% reduction in ONL thickness observed in GHL$^+$*rho*$^{+/-}$ retina and the 80% reduction observed in GHL$^+$*rho*$^{-/-}$ retina are consistent with accelerated degeneration occurring with transgene expression.

Fourth, the accelerated degeneration in GHL$^+$*rho*$^{-/-}$ retinas suggests inherent cytotoxicity of the mutant protein. In view of recent results in yeast and mammals, the cytotoxicity may be attributable to a UPR (reviewed in References 14,29,30). The UPR constitutes stress signaling from the ER lumen to the nucleus in response to accumulation of misfolded or unfolded polypeptides. By pathways imprecisely characterized in mammals, the UPR may induce transcription of additional chaperones (to assist folding), attenuation of translation (to prevent generation of more mutant protein), and mechanisms of protein degradation. Additional death-inducing signals are generated by the ER overload response (EOR). Also conceivable is that retention of mutant rhodopsin blocks the proteasome-ubiquitination pathway and thus triggers events culminating in apoptosis.[31] ER retention is a feature common to several well-characterized diseases (e.g., cystic fibrosis), in which the mutant chloride channel ΔF508-cystic fibrosis transmembrane conductance regulator (CFTR) misfolds and is unable to exit the ER.[32] Other examples in which misfolding of a nascent polypeptide chain leads to disease include neurodegenerative polyglutamine diseases (e.g., Huntington's disease), spinocerebellar ataxia (SCA), and spinobulbar muscular atrophy (SBMA), in which mutant proteins with poly(Q) expansions misfold, aggregate, misprocess, and gain cytotoxic functions not inherent to the normal proteins (reviewed in Reference 33).

Acknowledgments

The authors thank the laboratories of Helga Kolb and Robert Marc for expert advice and discussions, and Colin Barnstable and Robert Molday for generously providing rhodopsin antibodies.

References

1. Molday RS. Photoreceptor membrane proteins, phototransduction, and retinal degenerative diseases: The Friedenwald Lecture. *Invest Ophthalmol Vis Sci.* 1998;39:2491–2513.
2. Dryja TP, Li T. Molecular genetics of retinitis pigmentosa. *Hum Mol Genet.* 1995;4:1739–1743.
3. Inglehearn CF. Molecular genetics of human retinal dystrophies. *Eye.* 1998;12(Pt 3b):571–579.
4. Gregory-Evans K, Bhattacharya SS. Genetic blindness: current concepts in the pathogenesis of human outer retinal dystrophies. *Trends Genet.* 1998;14:103–108.
5. University of Texas-Houston Health Science Center. The Retina Network (RetNet). Available at http://www.sph.uth.tmc.edu/RetNet/disease.htm. Accessed January 19, 2001.
6. Dryja TP, McGee TL, Reichel E, et al. A point mutation of the rhodopsin gene in one form of retinitis pigmentosa. *Nature.* 1990; 343:364–369.
7. Olsson JE, Gordon JW, Pawlyk BS, et al. Transgenic mice with a rhodopsin mutation (Pro23His): a mouse model of autosomal dominant retinitis pigmentosa. *Neuron.* 1992;9:815–830.
8. Roof DJ, Adamian M, Hayes A. Rhodopsin accumulation at abnormal sites in retinas of mice with a human P23H rhodopsin transgene. *Invest Ophthalmol Vis Sci.* 1994;35:4049–4062.
9. Naash MI, Hollyfield JG, Al-Ubaidi MR, Baehr W. Simulation of human autosomal dominant retinitis pigmentosa in transgenic mice expressing a mutated murine opsin gene. *Proc Natl Acad Sci USA.* 1993;90:5499–5504.
10. Liu XR, Wu TH, Stowe S, et al. Defective phototransductive disk membrane morphogenesis in transgenic mice expressing opsin with a mutated N-terminal domain. *J Cell Sci.* 1997;110:2589–2597.
11. Sung C-H, Davenport CM, Nathans J. Rhodopsin mutations responsible for autosomal dominant retinitis pigmentosa: clustering of functional classes along the polypeptide chain. *J Biol Chem.* 1993; 268:26645–26649.
12. Humphries MM, Rancourt D, Farrar GJ, et al. Retinopathy induced in mice by targeted disruption of the rhodopsin gene. *Nat Genet.* 1997;15:216–219.
13. Lem J, Krasnoperova NV, Calvert PD, et al. Morphological, physiological, and biochemical changes in rhodopsin knockout mice. *Proc Natl Acad Sci USA.* 1999;96:736–741.
14. Kaufman RJ. Stress signaling from the lumen of the endoplasmic reticulum: coordination of gene transcriptional and translational controls. *Genes Dev.* 1999;13:1211–1233.

15. Laemmli UK. Cleavage of structural proteins during the assembly of the head of bacteriophage T4. *Nature.* 1970;227:680–685.
16. MacKenzie D, Arendt A, Hargrave P, McDowell JH, Molday RS. Localization of binding sites for carboxyl terminal specific anti-rhodopsin monoclonal antibodies using synthetic peptides. *Biochemistry.* 1984;23:6544–6549.
17. Frederick JM, Krasnoperova NV, Hoffmann K, Baehr W, Lem J, Rüther K. Retinal degeneration is accelerated when a mutant rhodopsin transgene is expressed on a haploid or null rhodopsin background. In: *Retinal Degenerative Diseases and Experimental Therapy.* New York: Kluwer Academic/Plenum; 1999;105–115.
18. Wada I, Rindress D, Cameron PH, et al. SSR alpha and associated calnexin are major calcium binding proteins of the endoplasmic reticulum membrane. *J Biol Chem.* 1991;266:19599–19610.
19. Al-Ubaidi MR, Pittler SJ, Champagne MS, Triantafyllos JT, McGinnis JF, Baehr W. Mouse opsin: gene structure and molecular basis of multiple transcripts. *J Biol Chem.* 1990;265:20563–20569.
20. Hargrave PA. Future directions for rhodopsin structure and function. *Behav Brain Sci.* 1995;18:403–414.
21. Colley NJ, Cassill JA, Baker EK, Zuker CS. Defective intracellular transport is the molecular basis of rhodopsin-dependent dominant retinal degeneration. *Proc Natl Acad Sci USA.* 1995;92:3070–3074.
22. Hebert DN, Simons JF, Peterson JR, Helenius A. Calnexin, calreticulin, and Bip/Kar2p in protein folding. *Cold Spring Har Symp Quant Biol.* 1995;60:405–415.
23. Ware FE, Vassilakos A, Peterson PA, Jackson MR, Lehrman MA, Williams DB. The molecular chaperone calnexin binds Glc1Man9GlcNAc2 oligosaccharide as an initial step in recognizing unfolded glycoproteins. *J Biol Chem.* 1995;270:4697–4704.
24. Molinari M, Helenius A. Chaperone selection during glycoprotein translocation into the endoplasmic reticulum. *Science* 2000;288:331–333.
25. Liu X, Garriga P, Khorana HG. Structure and function in rhodopsin: correct folding and misfolding in two point mutants in the intradiscal domain of rhodopsin identified in retinitis pigmentosa. *Proc Natl Acad Sci USA.* 1996;93:4554–4559.
26. Baker EK, Colley NJ, Zuker CS. The cyclophilin homolog NinaA functions as a chaperone, forming a stable complex in vivo with its protein target rhodopsin. *EMBO J.* 1994;13:4886–4895.
27. Ferreira PA, Nakayama TA, Pak WL, Travis GH. Cyclophilin-related protein RanBP2 acts as chaperone for red/green opsin. *Nature.* 1996;383:637–640.
28. Kurada P, Tonini TD, Serikaku MA, Piccini JP, O'Tousa JE. Rhodopsin maturation antagonized by dominant rhodopsin mutants. *Vis Neurosci.* 1998;15:693–700.
29. Pahl HL. Signal transduction from the endoplasmic reticulum to the cell nucleus. *Physiol Rev.* 1999;79:683–701.
30. Mori K. Tripartite management of unfolded proteins in the endoplasmic reticulum. *Cell.* 2000;101:451–454.
31. Plemper RK, Wolf DH. Retrograde protein translocation: eradication of secretory proteins in health and disease. *Trends Biochem Sci.* 1999;24:266–270.
32. Chang XB, Cui L, Hou YX, et al. Removal of multiple arginine-framed trafficking signals overcomes misprocessing of delta F508 CFTR present in most patients with cystic fibrosis. *Mol Cell.* 1999;4:137–142.
33. Lin X, Cummings CJ, Zoghbi HY. Expanding our understanding of polyglutamine diseases through mouse models. *Neuron.* 1999;24:499–502.
34. Danilczyk UG, Cohen-Doyle MF, Williams DB. Functional relationship between calreticulin, calnexin, and the endoplasmic reticulum luminal domain of calnexin. *J Biol Chem.* 2000;275:13089–13097.